

Dogfish egg case structural studies by ATR FT-IR and FT-Raman spectroscopy

Vassiliki A. Iconomidou^{a,1}, Martha E. Georgaka^{a,1}, Georgios D. Chryssikos^{b,2},
Vassilis Gionis^{b,2}, Persefoni Megalofonou^{c,3}, Stavros J. Hamodrakas^{a,*}

^a Department of Cell Biology and Biophysics, Faculty of Biology, University of Athens, Panepistimiopolis, Athens 157 01, Greece

^b Theoretical and Physical Chemistry Institute, National Hellenic Research Foundation, Athens 116 35, Greece

^c Department of Zoology and Marine Biology, Faculty of Biology, University of Athens, Panepistimiopolis, Athens 157 01, Greece

Received 17 November 2006; received in revised form 9 January 2007; accepted 9 January 2007

Available online 19 January 2007

Abstract

The dogfish egg case is a composite structure that combines mechanical tensile strength, toughness and elasticity with high permeability to small molecules and ions. Presumably, it provides both a protective and a filtering role for the egg/embryo contained within it. In this work, we performed structural studies of the *Galeus melastomus* egg case at two different stages of the hardening process, utilizing ATR FT-IR and FT-Raman spectroscopy. Based on these data we deduce that: (a) The *G. melastomus* egg case, in close analogy to that of the related species *Scyliorhinus canicula*, is a complex, composite structure which consists mainly of an analogue of collagen IV. This network forming protein appears to have common secondary structural characteristics in the entire egg case. (b) The outermost layer of the non-sclerotized egg case is especially rich in tyrosine, while the innermost layer is rich in polysaccharides, presumably glycosaminoglycans, and lipids. These differences are diminished upon hardening. (c) Disulfide bonds do not appear to play a significant role in cross-linking. However, cross-links involving tyrosine residues appear to sclerotize the egg case. It is proposed that the intensity of the Raman band at ca. 1615 cm⁻¹, which is due to ring stretching vibrations of Tyr, might be a useful indicator of the sclerotization status of a certain proteinaceous tissue, when tyrosines are involved in sclerotization mechanisms.

© 2007 Elsevier B.V. All rights reserved.

Keywords: Dogfish egg case; Analogue of collagen IV; ATR FT-IR spectroscopy; FT-Raman spectroscopy; Sclerotization; Structural study

1. Introduction

The selachian egg case is an elongated, leathery capsule ca. 50 mm by 20 mm (Fig. 1). It is a remarkable composite structure that combines mechanical tensile strength, toughness and elasticity with high permeability to small molecules and ions, thereby providing both a protective and a filtering role for the egg/embryo [1]. The egg case of the spotted dogfish, *Scyliorhinus canicula*, is constructed largely from collagen-containing fibrils with a unique crystalline arrangement [2–4]. The collagen

in these fibrils is secreted in a clearly defined zone (the D-zone), which forms the bulk of the nidamental gland [5–7]. Dogfish egg case collagen (DECC) is a network forming collagen, analogous to the mammalian collagen Types IV, VI, VIII and X [3,4,8–11,17]. The egg case of the spotted dogfish *S. canicula* is known to consist of four different layers (L₁–L₄) [1,2,7, see also Fig. 1]. The outermost layer (L₁), ca. 25 μm thick, contains hydrophobic protein granules 2 μm in diameter, exceptionally rich in tyrosine content (ca. 20%) and surrounded by radial arrangements of collagen fibrils [12]. The second layer (L₂), 225 μm thick, contains collagen, secreted mainly by the D-zone, as mentioned above, and comprises the main bulk of the egg case wall, in a unique plywood (helical) arrangement [1]. The third layer (L₃), 30 μm thick, contains also collagen but appears more homogeneous than the previous ones. Finally, a very thin (4–5 μm) innermost layer (L₄), contains mainly glycosaminoglycans and presumably collagen as well [2,7]. The presence of dopamine oxidase, DOPA, peroxidase and tyrosine-rich proteins

* Corresponding author. Tel.: +30 210 7274931; fax: +30 210 7274254.

E-mail addresses: veconom@biol.uoa.gr (V.A. Iconomidou), gdchryss@eie.gr (G.D. Chryssikos), pmegalo@biol.uoa.gr (P. Megalofonou), shamodr@biol.uoa.gr (S.J. Hamodrakas).

¹ Tel.: +30 210 7274931; fax: +30 210 7274254.

² Tel.: +30 210 7273819; fax: +30 210 7273820.

³ Tel.: +30 210 7274620; fax: +30 210 7274604.

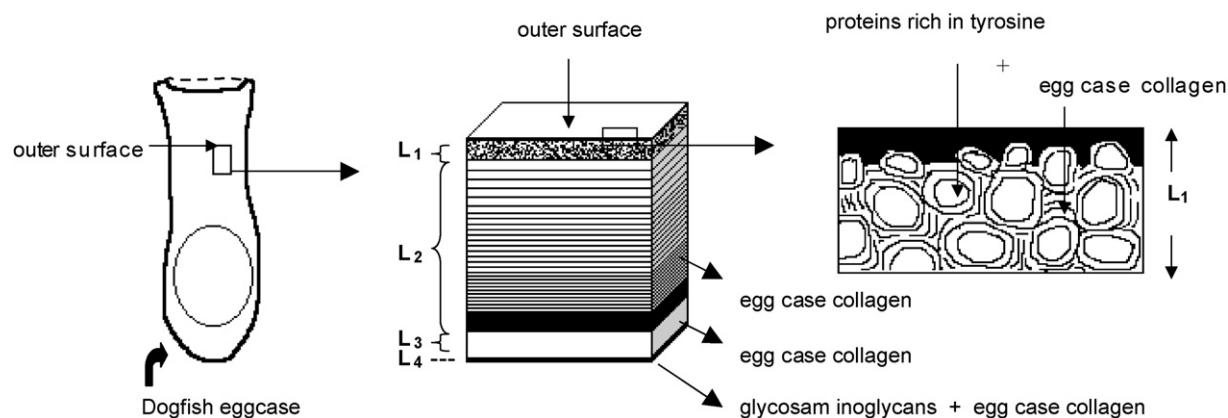


Fig. 1. A schematic drawing of the dogfish egg case, outlining its different layers and their protein content (adapted from [1,2]).

in the hydrophobic granules of L₁, suggests the possibility for extensive oxidative phenolic cross-linking but details of the sclerotization mechanisms are largely unknown [1,2,7].

The structures of the collagen assemblies in the egg case of the dogfish *S. canicula* have been studied previously using electron microscopy and 3D reconstruction [3,4,8,10,13–17] as well as X-ray diffraction [9,18,19]. From these studies, the collagen forming the bulk of egg case appears to assemble in layers of variable thickness, in which oriented quasi-crystalline fibers are laid down in approximately orthogonal directions systematically from one layer to another [1,2,20]. It is organized into a regular three-dimensional network with varying degrees of order [14–17]. The molecules of this sheet-forming collagen are approximately 45 nm long (reference [1] and references therein). Their packing arrangement is given in detail in references [14–17].

In this work we studied the wall of the egg case of another oviparous species, the blackmouth catshark, *Galeus melastomus* Rafinesque, 1810, which is classified under the Family Scyliorhinidae, like the species *S. canicula*, of the Class Elasmobranchii. *G. melastomus* is a deepwater bottom-dwelling shark, distributed in the eastern Atlantic Ocean, from Norway to Senegal, and in the whole Mediterranean Sea [21]. It shows a wide bathymetric range throughout the Mediterranean, in which it has been captured from depths of 55 to 1750 m. Egg deposition occurs all the year in the Mediterranean with a peak of activity in spring and summer. It lays up to 14 eggs at a time, which are left to grow without parental protection. The egg and the developing embryo are protected by an elongated leathery egg case (capsule), measuring ca. 6 cm by 3 cm or smaller in the Mediterranean population [22,23].

We have employed ATR FT-IR and FT-Raman spectroscopy to study two specimens of the egg case of *G. melastomus*, at different stages of hardening, in comparison to collagen IV, one of the known types of network forming collagens. Our aim was to study the secondary structure of the protein components of the dogfish egg case (DEC) and identify possible structural or compositional details related to the sclerotization mechanism(s). To our knowledge, this is the first detailed vibrational spectroscopic investigation of a selachian egg case.

2. Materials and methods

2.1. Materials

Two egg cases, at different stages of hardening, were obtained from a single female shark of the species *G. melastomus*. The egg cases were flattish rectangular pouches of some 6 cm × 3 cm. One was newly formed in the vicinity of the nidamental gland and was white in color. The other egg case was obtained from the oviduct and was brown. Both DEC samples were cut in half along their longest dimension, washed with distilled water briefly in a sonicator to remove remnants, and then stored immersed in distilled water at 4 °C. The DEC samples have been studied fresh, because prolonged storage was found to change the colouring of the specimens: the white egg case gradually acquired a yellowish to brown colour. Small square (5 mm × 5 mm) or round (2 mm in diameter) pieces were cut from the midsection of the egg case wall, left to dry in ambient conditions and used immediately for the ATR FT-IR and Raman measurements. Care was taken to mark the orientation (inner, in contact with the egg and the developing embryo, or outer surfaces, see Fig. 1) of the specimens where needed (ATR FT-IR spectroscopy).

Dry powdered collagen IV from human placenta was purchased from Sigma–Aldrich (C-7521) and used as received.

2.2. Attenuated total reflectance infrared spectroscopy (ATR FT-IR)

Infrared spectra were obtained with an IR microscope (IRScope II by Bruker Optics) equipped with a Ge attenuated total reflectance objective lens (ATR 20×) and attached to a Fourier-transform spectrometer (Equinox 55 by Bruker Optics). Small (5 mm × 5 mm) pieces of the egg cases were placed on a front coated Au mirror and the ATR spectra were measured by bringing the Ge-element in contact with their exposed surface. The corresponding spectrum of collagen IV was obtained from the neat powder. The use of the ATR technique was imposed by the thickness of the DEC samples (ca. 300 μm) that does not allow for measurements in transmission, as well as from the requirement for non-destructive characterization [24]. With

a penetration depth of less than $1 \mu\text{m}$ (1000 cm^{-1} , Ge), ATR is free of saturation effects and probes exclusively the external layers of the egg case. All spectra are obtained at 4 cm^{-1} resolution, represent averages of ca. 300 scans, and are shown in the ATR absorption formalism, i.e. after correction for the wavelength-dependence of the penetration depth ($d_p \propto \lambda$).

2.3. Fourier transform (FT)-Raman spectroscopy

The Raman spectra were obtained on a Fourier transform instrument (RFS 100 by Bruker Optics) employing for excitation ca. 400 mW of the Nd:YAG 1064 nm line in a backscattering geometry. Due to differences in the vibrational selection rules, Raman scattering provides information complementary to infrared absorption. Excitation in the near infrared reduces significantly the fluorescence of the proteinaceous samples and eliminates the need for prolonged laser annealing. Several disks (2 mm in diameter) were cut from the egg case and placed in the cavity of a standard aluminum holder. Due to the large scattering volume, no effect of the sample orientation (inner side up or down) was observed in the spectra, and the latter should be taken as representing the average structure of the samples. The spectra have been measured at a resolution of 4 cm^{-1} and represent averages of ca. 5000–8000 scans. The Raman spectrum of collagen IV was obtained under the same conditions by pressing the dry powder of collagen IV from human placenta into the 2 mm cavity of a standard aluminum holder.

2.4. Post-run computations of the spectra

All spectra have been collected with a zero filling factor of 2. In order to enhance the resolution of sharp features overlapping with broad bands, the Raman scattering and infrared ATR absorption peak maxima were determined also from the minima in the second derivative of the corresponding spectra. Derivatives were computed analytically by the Savitsky–Golay algorithm [25] using routines of the OPUS software (Bruker Optics) and included a 9 (ATR) or 13 (Raman) point smoothing. Smoothing over narrower ranges resulted to a deterioration of the S/N ratio and did not increase the number of minima that could be determined with confidence.

3. Results and discussion

3.1. ATR FT-IR spectroscopy

The ATR FT-IR spectra of the white and brown DEC specimens measured from their outer and inner surfaces are shown in Fig. 2, in comparison to the corresponding spectrum of collagen IV. All spectra correspond to materials at similar hydration states, as revealed by the similar intensity of the water stretching bands (not shown). The corresponding second derivative spectra are shown in Fig. 3, and the peak positions determined from the minima of the derivative spectra are compiled in Table 1. Table 1 also includes for comparison absorption band maxima of various tissues containing collagen IV obtained from the literature, as well as suggested assignments.

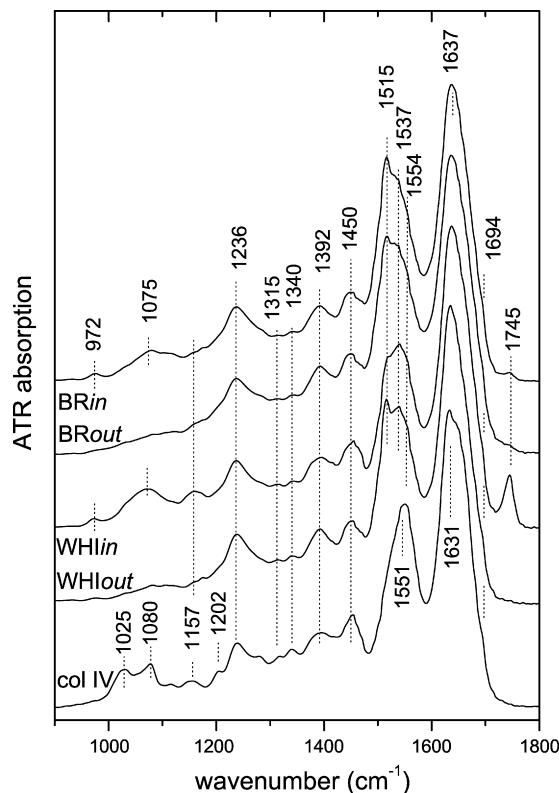


Fig. 2. Attenuated total reflectance FT-infrared (ATR FT-IR) spectra of white (WHI) and brown (BR) *G. melastomus* egg case specimens, measured from the inner (*in*) and outer (*out*) surfaces, in comparison to the spectrum of collagen IV (col IV). Peaks are labelled as absorption maxima. The spectra have been offset for clarity.

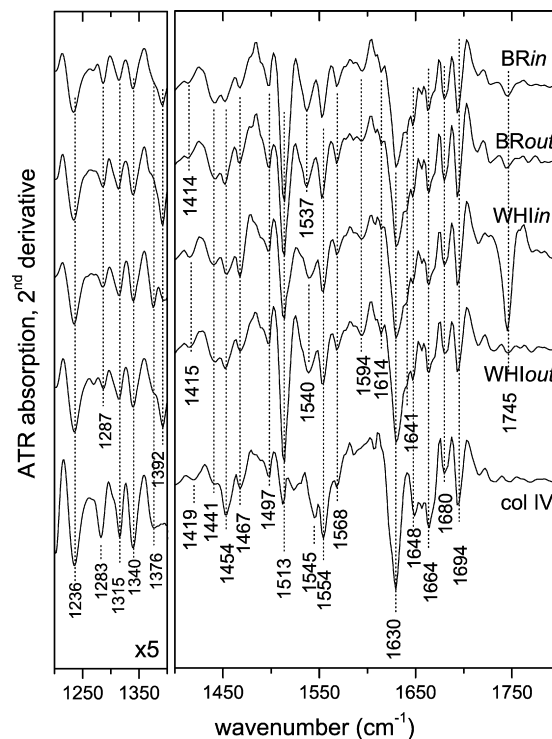


Fig. 3. Second derivatives of the spectra of Fig. 2. Peaks are labelled as minima and compiled in Table 1.

Table 1

Main ATR FT-IR (1200–1800 cm^{-1}) peak positions determined from the minima of the second derivative spectra of: (a) *G. melastomus* egg case (this work), (b) collagen IV (this work) and, also, ATR FT-IR absorption band maxima from: (c) collagen IV from vascular graft [28], (d) aqueous solution of collagen IV from human placenta [26], (e) aqueous solution of collagen IV from human placenta [27]

Dogfish egg case collagen, this work	Powder collagen IV from human placenta, this work	Collagen IV from vascular graft [28]	Aqueous solution of collagen IV [26]	Aqueous solution of collagen IV [27]	Assignments-comments
1745					Mostly in the inner layer of white DEC, lipids
1694	1694				Amide I, β -turns
1680	1680				Amide I, β -turns
1664	1664				Amide I, β -turns
1648	1648	1653	1650	1647	Amide I, triple helix as in Col I; α -helix, random coil?
1641					Amide I, note: absent from our col IV
1630	1630	1632	1633	1633	Amide I, collagen IV, note: at lower resolution this peak shifts up towards 1633, as in the literature for col IV
1614					Tyr, v. weak (Raman active)
1594					COO ⁻ end groups, broad
1568	1568				
1554	1554		1554		Amide II, collagen IV
1540	1545	1544		1545	Amide II, collagen IV, 1537 cm^{-1} in brown DECs, note: shifts systematically upon sclerotization
1513	1513				Tyr, v. strong in DECs, weak in col IV
1497	1497				
1467	1467				CH ₂ scissoring (also due to lipids)
1454	1454	1455	1456	1456	CH ₂ scissoring
1441	1441				CH ₂ scissoring?, weak in col IV
1415	1419				CH ₃ deformation, 1413 in brown DECs, note: shifts systematically upon sclerotization
1392	1400		1403	1398	CH ₂ deformation, symmetric stretching of COO ⁻ , C–N stretching?
1376	1376				
1340	1340	1340		1338	C–H wag,
1315	1315				C–H wag,
1287	1283			1283	Amide III, collagen IV
1236	1236	1238	1242	1244	Amide III, collagen IV

Tentative assignments and comments are included. For details see text.

When compared in the second derivative formalism, collagen IV and the DEC specimens, white or brown, outer or inner, exhibit many similarities in the amide I, II and III regions, suggesting the existence of common secondary structural characteristics. In all spectra, the strongest amide I band is observed at 1630 cm^{-1} and is accompanied by a number of weaker components at higher frequencies (Fig. 3). The amide II region is dominated by bands at 1568, 1554 and ca. 1540 cm^{-1} . Finally, the amide III region of all samples includes bands at 1340, 1315 and ca. 1285 and 1236 cm^{-1} .

Beyond these similarities, several spectral differences are of interest: first we note that the spectra of the DEC specimens all involve a very strong absorption at 1513 cm^{-1} that is nearly absent from the spectrum of collagen IV. In agreement with [29] we attribute this band to the semicircle C=C stretching of tyrosine rings. The corresponding quadrant stretching is observed at 1614 cm^{-1} (Fig. 3) with very low infrared activity due to the *para* substitution. Additional differences between DEC and collagen IV can be seen in the 900–1100 cm^{-1} range of the absorption spectra (Fig. 2). Collagen IV exhibits two broad bands at ca. 1025 and 1080 cm^{-1} attributed to proteoglycans (26, 27, 30),

but the inner DEC layers show a sharp band at 972 cm^{-1} , and a broader envelope centered at 1075 cm^{-1} . Both these latter features are typical of polysaccharides [30,31], but these appear to be different than those associated with collagen IV.

Further, we note that the spectrum of the inner layer of the white DEC (and to a lesser extent the corresponding spectrum of the brown DEC) exhibit a pronounced C=O stretch at 1745 cm^{-1} (Figs. 2 and 3). The intensity of this band parallels the intensity of sharp C–H stretching features at 2853, 2924, 2961 and 3011 cm^{-1} (not shown), as well as the intensity enhancement of the CH₂ scissoring mode at 1467 cm^{-1} . Clearly, these features should be attributed to the presence of *cis*-unsaturated lipids in the inner layer of the DEC, especially during the early stages from its formation [32].

Apart from the presence of polysaccharides, presumably glycosaminoglycans [2,7], and lipids in the inner layer of the DECs, very few differences can be observed between the ATR spectra of the white and brown egg cases. Among them, we note that the intensity of the 1513 cm^{-1} tyrosine band is considerably lower in the outer layer of the brown egg case than in the corresponding white specimen (Figs. 2 and 3). Parallel small but

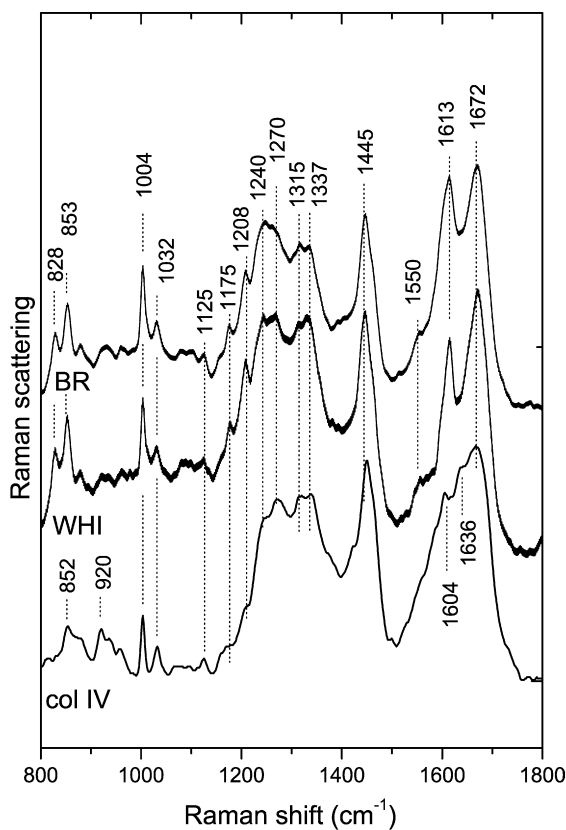


Fig. 4. FT-Raman spectra of white (WHI) and brown (BR) *G. melastomus* egg case specimens and collagen IV (col IV). Peaks are labelled as scattering maxima. The spectra have been offset for clarity.

systematic shifts are observed in two weak bands from 1415 and 1540 cm^{-1} (white DEC, Fig. 2) to 1414 and 1537 cm^{-1} (brown DEC). Though a more quantitative analysis of these trends is not possible due to the overlap of the tyrosine with the amide II envelope, the dependence of the intensity of the semicircle ring stretching modes on the electron donor properties of the substituent $-\text{OH}$ group, as well as the unknown assignments of the 1415 and 1540 cm^{-1} features, we advance the hypothesis that these may be indicative of progressing sclerotization involving the tyrosine groups.

Although it is difficult to judge the relative amounts of Tyr in the proteins of the two surface layers due to overlap of the 1513 cm^{-1} band with the amide II band, it is worth noting that in the white specimen, the outer layer appears enriched in Tyr, in agreement with the literature concerning the hydrophobic granules of the outermost L_1 layer (see Section 1 and references therein and also Fig. 1). On the contrary, in the brown egg case, this trend appears reversed, and this could be taken as an indirect manifestation of cross-linking.

3.2. FT-Raman spectroscopy

The Raman spectra obtained from the white and brown DEC specimens are shown in Fig. 4, together with the spectrum of collagen IV. The corresponding second derivative spectra are shown in Fig. 5, while the Raman peak positions determined

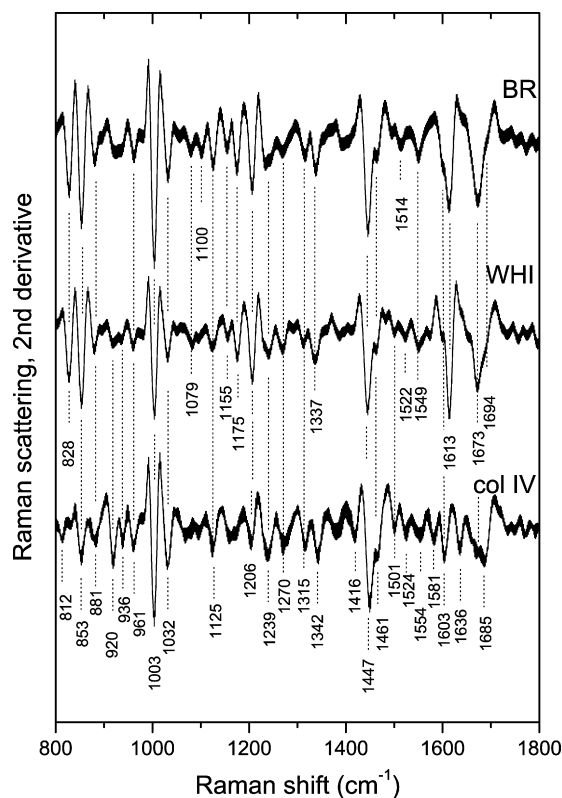


Fig. 5. Second derivatives of the FT-Raman spectra shown in Fig. 4. Peaks are labelled as minima and compiled in Table 2.

from the minima of the second derivatives, are compiled in Table 2.

In the amide I region both DEC's exhibit sharp Raman bands at 1673 cm^{-1} (which is the Raman counterpart of the infrared active amide I component at 1630 cm^{-1}) with a higher frequency shoulder at ca. 1695 cm^{-1} . Two peaks can be discerned by second derivative analysis in the amide III region, at 1239 and 1270 cm^{-1} . As in the case of the ATR spectra, the low wavenumber component of the amide III doublet is a common vibrational characteristic feature of proteins adopting β -sheet structure. However, we note that the spectrum of collagen IV also exhibits an amide III doublet at 1239 and 1270 cm^{-1} . A similar splitting of the amide III band was also reported for collagen I and was attributed to the proline-poor (polar) and proline-rich (non polar) regions distributed along the triple helix [33–35]. The amide I Raman spectrum of collagen IV exhibits three poorly resolved component bands at 1636, 1673 and 1685 cm^{-1} (Figs. 4 and 5), while the published spectrum of collagen I shows the main amide I component at ca. 1670 cm^{-1} , and a shoulder at 1642 cm^{-1} [33].

It is known that collagen IV is structurally different from collagen I in a number of aspects. First, it is not of a straight triple-helical type, but it rather has kinks along the triple helix, most probably due to disruptions of the regular Gly-X-Y repeats along its sequence. Second, it contains C-terminal globular non-collagenous domains (NC1 domains), whose structure has been solved near atomic resolution (1.9 Å), where β -sheet conformation prevails [36]. Further, the DEC collagen, though analogous

Table 2
Main Raman band maxima (800–1800 cm⁻¹) determined from the minima of the second derivative spectra

<i>G. melastomus</i> white egg case (cm ⁻¹)	<i>G. melastomus</i> brown egg case (cm ⁻¹)	Collagen IV (cm ⁻¹)	Assignment
1694	1694	1685	Amide I, collagen IV
1673	1673	1673	Amide I, collagen IV
		1636	Amide I, collagen IV
1613	1613		Tyr
		1603	Phe
		1581	Pro, hydro
1549	1549	1554	Amide II, collagen IV
1522	1514	1524	Tyr
		1501	
1461	1461	1461	CH ₂ deformation
1447	1447	1447	CH ₂ deformation
		1416	COO ⁻ symmetric stretching
1337	1337	1342	Trp, CH deformation
1315	1315	1315	CH deformation
1270	1270	1270	Amide III, collagen IV
1239	1239	1239	Amide III, collagen IV
1206	1206	1206	Tyr, Phe
1175	1175		Tyr
1155	1155	1160	C–N stretching
1125	1125	1125	C–N, C–C stretching
1079	1079		C–C, C–O stretching
1032	1032	1032	Phe, C–C, C–O stretching
1003	1003	1003	Phe
961	961	961	C–C stretching
936		936	C–C stretching of protein backbone
920		920	C–C stretching of Pro ring
881	881	881	Trp
853	853	852	Tyr
828	828		Tyr
		812	C–C stretching of backbone

Tentative assignments are included. For details see text.

to mammalian collagen IV, is only 45 nm long (compared to 400 nm of mammalian collagen IV) and terminates, at both ends, with two hydrophobic globular domains about 4 and 2 nm in diameter [1,6]. These structural characteristics should account for the observed differences between the Raman spectra of collagen I and IV, as well as for the structural differences between mammalian collagen I and egg case collagen.

The FT-Raman spectra of both white and brown DEC specimens exhibit several bands which are clearly due to side chain vibrations of aminoacid residues, especially to the aromatic ring-containing Tyr, Phe and Trp (Figs. 4, 5 and Table 2). More specifically, the bands at 1003 and 1032 cm⁻¹ are ascribable to Phe, whereas the bands at 828, 853, 1175, 1206 and 1613 cm⁻¹ are most likely due to Tyr [37–39]. The presence of these aromatic residues is also confirmed by characteristic bands in the 600–800 cm⁻¹ range (not shown). The intensity ratio of the tyrosine doublet at 853 and 828 cm⁻¹, $R = I_{853}/I_{828}$, is sensitive to the nature of hydrogen bonding or to the state of the ionization of the phenolic hydroxyl group, and has been used to identify “buried” and “exposed” Tyr moieties [40]. For both, white and brown egg cases, $R \sim 1.3$ indicating that the phenolic hydroxyl group may be involved in moderate hydrogen bonds (reference [40] and references therein). The 1206 cm⁻¹ band may also involve contributions from vibrations of Phe. Also, the band at 1613 cm⁻¹ may hide components due to Phe and Trp. The absence of a band at 1361 cm⁻¹ sug-

gests presumably that the Trp side chains are not “exposed” [38].

Of particular interest is the observation that in the brown DEC specimen there is a significant broadening of the 1613 cm⁻¹ band compared the newly formed white DEC (Fig. 4). This broadening is manifested as a decreasing intensity of the second derivative spectrum (Fig. 5). Since this band is associated with the presence of Tyr [29], its broadening in the sclerotized DEC may signal structural changes relevant to the oxidative phenolic tanning reactions (reference [1] and references therein). The involvement of Tyr in cross-linking reactions that harden the egg case is particularly appealing since the Raman spectra do not provide evidence for another common cross-linking mechanism, namely the formation of disulfide bonds. The latter are characterized by well-defined Raman features at 510, 525 and 540 cm⁻¹ [37–39], but these are not observed in the spectra of the egg cases (data not shown).

4. Conclusions

The egg case of dogfish and related species is a complex composite with extraordinary mechanical and functional properties. This combined ATR FT-IR and FT-Raman study of the *G. melastomus* egg case confirms the observations from EM studies and biochemical data on the egg case of the related species *S. canicula*, about a different distribution of components in the different

layers of the egg case wall. It clearly shows the preponderance of proteins rich in Tyr in the outermost surface layers of the egg case and the presence of glycosaminoglycans and unsaturated lipids in the innermost layers.

Concerning the cross-linking mechanisms, we found no Raman evidence for the formation of disulfide bridges in the sclerotized egg case. Instead, the careful spectral comparison of the new and sclerotized cases revealed changes in features attributed to tyrosines that are compatible with the formation of di-tyrosine and tri-tyrosine cross-links [1,42,43]. Interestingly, similar changes involving the vibrational spectrum of Tyr were observed in a study of insect cuticle sclerotization (Iconomidou, Chryssikos, Gionis, Willis and Hamodrakas, unpublished data).

Furthermore, the analysis of the vibrational spectra of the egg cases and their comparison to the corresponding spectra of the mammalian collagen IV, one of the known network forming collagens, suggests that the main protein component of the egg case exhibits a secondary structure similar but not identical to that of collagen IV. The similarities between the two types of collagen appear to involve spectral characteristics that are normally associated with β -sheet conformations in both fibrous and globular proteins, including those that constitute the non-collagenous egg chorions of insects and teleostean fish [41,44]. At present, we tend to attribute these similarities to the non-collagenous domains, which have been documented to contain abundant β -sheet at least in the case of mammalian collagen IV [36]. However, a thorough vibrational investigation of the whole family of network forming collagens is needed in order to identify those common structural characteristics that relate to their unique biological and materials properties. It is true that DECC is more similar, at least in packing arrangement, to collagen VI rather than collagen IV [17].

Acknowledgements

Financial support for this work was provided by the University of Athens. Additional support was provided through funds of the Applied Spectroscopy Lab of TPCI/NHRF. We would like to thank the reviewers of this manuscript for their useful and constructive criticism.

References

- [1] D.P. Knight, D. Feng, M. Stewart, *Biol. Rev.* 71 (1996) 81.
- [2] M. Rusaouën, J.-P. Puzol, J. Bocquet, A. Veillard, J.-P. Borel, *Comp. Biochem. Physiol.* 53B (1976) 539.
- [3] D.P. Knight, S. Hunt, *Tissue Cell* 8 (1976) 183.
- [4] D.P. Knight, S. Hunt, *Tissue Cell* 18 (1986) 201.
- [5] M. Rusaouën-Innocent, *Can. J. Zool.* 68 (1990) 2553.
- [6] M. Rusaouën-Innocent, *Tissue Cell* 22 (1990) 449.
- [7] D. Feng, D.P. Knight, *Tissue Cell* 24 (1992) 773.
- [8] D.P. Knight, S. Hunt, *Nature* 249 (1974) 379.
- [9] L.J. Gathercole, E.D.T. Atkins, E.G. Goldbeck-Wood, K. Barnard, *Int. J. Biol. Macromol.* 15 (1993) 81.
- [10] D.P. Knight, D. Feng, *Tissue Cell* 26 (1994) 385.
- [11] T.-T. Luong, M.-M. Boutillon, R. Garrone, D.P. Knight, *Biochem. Biophys. Res. Commun.* 250 (1998) 657.
- [12] D.P. Knight, D. Feng, *Tissue Cell* 26 (1994) 155–167.
- [13] D.P. Knight, D. Feng, M. Stewart, E. King, *Phil. Trans. R. Soc. Lond. B* 341 (1993) 419.
- [14] C. Knupp, M. Chew, E. Morris, J. Squire, *J. Struct. Biol.* 117 (1996) 209.
- [15] C. Knupp, M. Chew, J. Squire, *J. Struct. Biol.* 122 (1998) 101.
- [16] C. Knupp, P.K. Luther, E.P. Morris, D.P. Knight, J.M. Squire, *J. Struct. Biol.* 126 (1999) 121.
- [17] C. Knupp, J.M. Squire, *Adv. Protein Chem.* 70 (2005) 375.
- [18] D.G. Hepworth, L.J. Gathercole, D.P. Knight, D. Feng, J.F.V. Vincent, *J. Struct. Biol.* 112 (1994) 231.
- [19] C. Knupp, J. Squire, *Proc. R. Soc. Lond. B* 265 (1998) 2177.
- [20] D.P. Knight, D. Feng, *J. Biomim.* 1 (1992) 151.
- [21] L.J.V. Compagno, *FAO species catalogue, Vol. 4: sharks of the world: an annotated and illustrated catalogue of shark species known to date. Part 2. Carchariniformes. FAO Fish Synopsis* 1984, pp. 125, 251.
- [22] A. Tursi, G. d'Onghia, A. Matarrese, G. Piscitelli, *Cybiurn* 17 (1993) 187.
- [23] M.E. Costa, K. Erzini, T. Borges, *J. Mar. Biol. Assoc. UK* 85 (2005) 1173.
- [24] H.H.J. de Jongh, E. Goormaghtigh, J.M. Ruyschaert, *Anal. Biochem.* 242 (1996) 95.
- [25] A. Savitsky, M.J.E. Golay, *Anal. Chem.* 36 (1964) 1627.
- [26] Y. Ozaki, A. Mizuno, F. Kaneuchi, *Appl. Spectrosc.* 46 (1992) 626.
- [27] S.-M. Lee, S.-Y. Lin, R.-C. Liang, *Artif. Cells Blood Substit. Immobil. Biotech.* 23 (1995) 193.
- [28] D.J. Lyman, J. Murray-Wijelath, *J. Biomed. Mater. Res.* 48 (1999) 172.
- [29] S. Krimm, J. Bandekar, *Adv. Protein Chem.* 38 (1986) 181.
- [30] M. Khajehpour, J.L. Dashnau, J.M. Vanderkooi, *Anal. Biochem.* 348 (2006) 40.
- [31] M. Mathlouthi, J.L. Koenig, *Adv. Carbohydr. Chem. Biochem.* 44 (1986) 7.
- [32] S. Yoshida, H. Yoshida, *Biopolymers* 74 (2004) 403.
- [33] B.J. Frushour, J.L. Koenig, *Biopolymers* 14 (1975) 379.
- [34] S.C. Goheen, L.J. Lis, J.W. Kauffman, *Biochim. Biophys. Acta* 536 (1978) 197.
- [35] T. Ikoma, H. Kobayashi, J. Tanaka, D. Walsh, S. Mann, *Int. J. Biol. Macromol.* 32 (2003) 199.
- [36] M.E. Than, S. Henrich, R. Huber, A. Ries, K. Mann, K. Kühn, R. Timpl, G.P. Bourenkov, H.D. Bartunik, W. Bode, *Proc. Natl. Acad. Sci. U.S.A.* 99 (2002) 6607.
- [37] B.J. Frushour, J.L. Koenig, in: R.J.H. Clark, R.E. Hester (Eds.), *Advances in Infrared and Raman Spectroscopy*, Heyden, London, 1975, p. 35.
- [38] N.T. Yu, *CRC Crit. Rev. Biochem.* 4 (1977) 229.
- [39] T.G. Spiro, B.P. Gaber, *Annu. Rev. Biochem.* 46 (1977) 553.
- [40] P.R. Carey, *Biochemical Applications of Raman and Resonance Raman Spectroscopies*, Academic Press, New York, 1982.
- [41] S.J. Hamodrakas, S.A. Asher, G.D. Mazur, J.C. Regier, F.C. Kafatos, *Biochim. Biophys. Acta* 703 (1982) 216.
- [42] S.O. Andersen, in: L. Gilbert, K. Iatrou, S. Gill (Eds.), *Comprehensive Molecular Insect Science*, Elsevier, Oxford, 2005, p. 145.
- [43] T.L. Hopkins, K.J. Kramer, *Annu. Rev. Entomol.* 37 (1992) 273.
- [44] V.I. Iconomidou, D.G. Chryssikos, V. Gionis, M.A. Pavlidis, A. Paipetis, S.J. Hamodrakas, *J. Struct. Biol.* 132 (2000) 112.